






Thermodynamic properties of the Mott insulator-metal transition in a triangular lattice system without magnetic order

Emre Yesil ¹, Shusaku Imajo ^{2,*}, Satoshi Yamashita ¹, Hiroki Akutsu¹, Yohei Saito ³, Andrej Pustogow ⁴,
Atsushi Kawamoto⁵ and Yasuhiro Nakazawa^{1,†}

¹Graduate School of Science, Osaka University, Toyonaka, Osaka 560-0043, Japan

²Institute for Solid State Physics, University of Tokyo, Kashiwa, Chiba 277-8581, Japan

³Institute of Physics, Goethe-University Frankfurt, 60438 Frankfurt am Main, Germany

⁴Institute of Solid State Physics, TU Wien, 1040 Vienna, Austria

⁵Graduate School of Science, Hokkaido University, Sapporo 060-0810, Japan



(Received 23 June 2022; revised 29 October 2022; accepted 9 January 2023; published 23 January 2023)

The organic system κ -[(BEDT-TTF)_{1-x}(BEDT-STF)_x]₂Cu₂(CN)₃, showing a Mott transition between a nonmagnetic Mott insulating (NMI) state and a Fermi liquid (FL), is systematically studied using calorimetric measurements. An increase in the electronic heat capacity at the transition from the NMI state to the FL state which keeps the triangular dimer lattice demonstrates that the charge sector lost in the Mott insulating state is recovered in the FL state. We observed that the remaining low-energy spin excitations in the Mott insulating state show a unique temperature dependence and that the NMI state has a larger lattice entropy originating from the frustrated lattice, which leads to a Pomeranchuk-like effect on the electron localization. Near the Mott boundary, an unexpected enhancement and magnetic field dependence of the heat capacity are observed. This anomalous heat capacity is different from the behavior in a typical first-order Mott transition and shows similarities with quantum critical behavior. To reconcile our results with previously reported scenarios about a spin gap and the first-order Mott transition, further studies are desired.

DOI: [10.1103/PhysRevB.107.045133](https://doi.org/10.1103/PhysRevB.107.045133)

I. INTRODUCTION

The dimer-Mott compounds with the chemical formula of κ -(BEDT-TTF)₂X, where BEDT-TTF is bis(ethylenedithio)tetrathiafulvalene and X is a monovalent counter anion, provide extensive possibilities for understanding physical phenomena induced by electron correlations of π electrons [1,2]. Electrons in them form relatively narrow electron bands governed by overlaps of molecular orbitals, and the spin, charge, and lattice degrees of freedom appear in various manners in them. The electronic states of the dimer-Mott system can be described in the frame of the Mott-Hubbard physics with on-site Coulomb repulsion U and bandwidth W (proportional to transfer integral t) [1–5]. Additionally, the dimer lattice of the κ -type molecular arrangement has geometrical frustration depending on the ratio of t and t' , nearest-neighbor and second-nearest-neighbor transfer integrals, as shown in Fig. 1(a). Using the two parameters U/t vs t'/t , the electronic phase diagram has been understood, as shown in Fig. 1(b) [6,7]. For the less-frustrated salts ($t'/t < 1$), the discontinuity and hysteresis in the electrical transport indicate that the superconductivity–antiferromagnetic-insulator (SC-AFMI) transition dominated by a change in U/t [the light blue arrow in Fig. 1(b)] is first order [8–12].

As schematically described in Fig. 1(c), the first-order Mott boundary disappears at a critical endpoint of ~ 35 K, and the nature of the Mott physics around the endpoint has been discussed in terms of high-energy criticality caused by the competition between the large U and $W > 1000$ K [10–12]. From the antiferromagnetic (AFM) order induced by antiferromagnetic interactions, the SC with relatively high T_c has been extensively discussed in terms of unconventional pairing related to antiferromagnetic spin fluctuations in κ -(BEDT-TTF)₂X and also in β' -, λ -type compounds [13–17]. The variation in physical parameters near the Mott boundary has been studied by various measurements across the boundary [18–22]. Based on the variation in the electronic heat capacity coefficient γ of the normal state shown in Fig. 1(c) [14,23–26], the low-temperature Fermi liquid (FL) state can be understood by the electron-mass enhancement with increasing electron correlations (the green arrow) and the decrease in the metallic portion due to the growth of phase coexistence near the Mott boundary (the orange arrow). Although slight percolative superconductivity is left in the AFM Mott insulating salts very near the boundary, its γ is almost zero because the volume fraction of the FL is negligible. It should be noted that the information contains the magnetic entropy change related to the AFMI ground state of π electrons and that the change is not a genuine feature expected in the Hubbard model because no symmetry breaking is assumed in this framework [27–31]. When $t'/t = 1$, the AFMI ground state should be destabilized by the geometrical frustration, and nonordered states may be stable

*imajo@issp.u-tokyo.ac.jp

†nakazawa@chem.sci.osaka-u.ac.jp

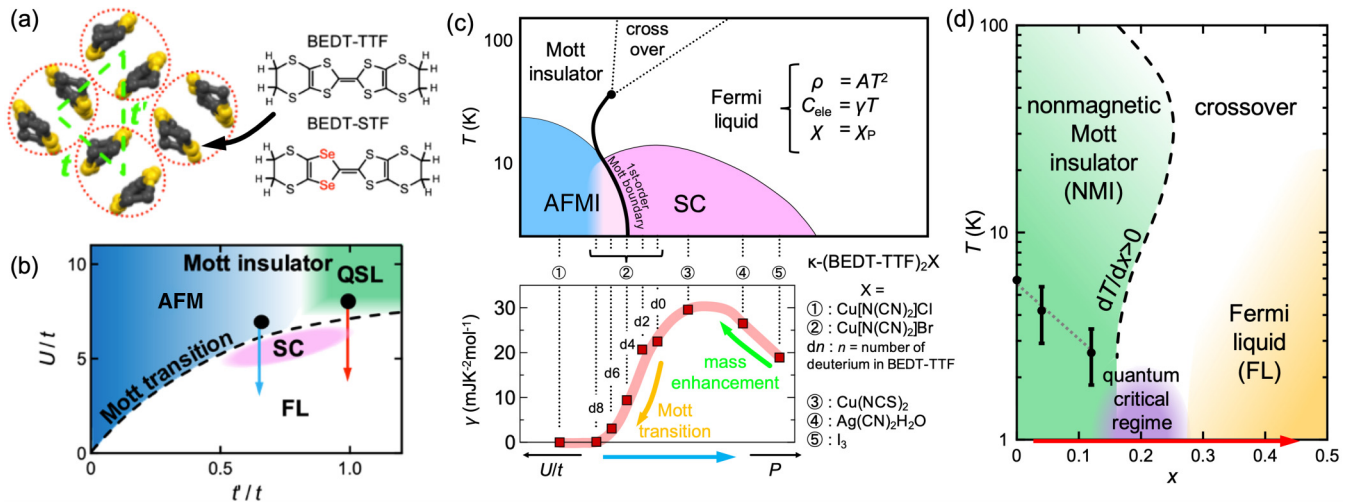


FIG. 1. (a) Molecular arrangement in the conducting plane of the present system and BEDT-TTF and BEDT-STF molecules. t and t' indicate nearest-neighbor and second-nearest-neighbor transfer integrals in the dimer lattice, respectively. (b) Electronic ground states of the dimer-Mott system with parameters of electron correlations U/t (U/W) and frustration factor t'/t [6,7]. The red arrow indicates the route controlled by substitution in the present system, whereas the light blue arrow represents the numerous previous studies on the less-frustrated dimer-Mott system. (c) Electronic phase diagram of the less-frustrated κ -type salts with the shown counteranions. The AFMI and FL phases are divided by the first-order Mott transition, which terminates at a critical endpoint ~ 35 K. Inside the FL, SC with relatively high T_c , ~ 10 K, occurs near the boundary. The lower panel shows the variation in γ of the normal state depending on electron correlations U/t and chemical pressure of the counteranion P . (d) Schematic phase diagram of κ -[(BEDT-TTF) $_{1-x}$ (BEDT-STF) $_x$] $_2$ Cu $_2$ (CN) $_3$ deduced from Refs. [36–39]. An increase in the mixing ratio x corresponds to a decrease in U/t shown by the red arrow in the phase diagram (b). The NMI and electronic FL states exist across the quantum critical regime, which is located around $x = 0.2$. The dashed curve indicates the phase boundary between the NMI and FL phases; its slope dT/dx is positive at low temperature. The black dots in the NMI region represent the x dependence of the so-called 6-K anomaly, in which error bars are determined by the present heat capacity measurements.

even at low temperatures. Indeed, κ -(BEDT-TTF) $_2$ Cu $_2$ (CN) $_3$, which has been considered a prime candidate showing the quantum spin liquid (QSL) state, does not show long-range magnetic orders down to extremely low temperatures because t'/t is almost unity [32,33]. However, recently, Miksch *et al.* [34] and Pustogow [31] suggested that its ground state might be a gapped valence bond solid (VBS) with a spin gap from observation of a drop of spin susceptibility below 6 K. Although the controversy still persists because of the remaining discrepancy with the gapless spin excitations in heat capacity [35], we hereinafter use the term “nonmagnetic Mott insulating” (NMI) for describing the Mott insulating state.

Recently, Saito and co-workers reported that a donor alloying system of (BEDT-TTF) $_{1-x}$ (BEDT-STF) $_x$, where BEDT-TTF and BEDT-STF are the abbreviations of bis(ethylenedithio)tetrathiafulvalene and bis(ethylenedithio)diselenadithiafulvalene, with Cu $_2$ (CN) $_3$ exhibits continuous tuning of U/W while keeping the triangularity of the dimer lattice [36–39]. The Se substitution into the BEDT-TTF molecule shown in Fig. 1(a) results in a larger overlap of the wave function with the neighboring molecules. Since the increase in x is considered to work as positive chemical pressure without inducing a large change in average t'/t , the insulating state is altered into the FL state via the genuine Mott transition at $x = 0.1$ – 0.2 [36–39], as indicated by the red arrow in Fig. 1(b). This variation is similar to the tuning by external pressure to κ -(BEDT-TTF) $_2$ Cu $_2$ (CN) $_3$ where the ground state without magnetic order shifts to a FL across the Mott-insulator–metal

transition [8,9]. Namely, this variation provides profound information on the Mott transition genuinely dominated by the itinerancy or localization of the charge degrees of freedom. The T - x electronic phase diagram of the present alloying system is predicted from the results in Refs. [36–39], as shown in Fig. 1(d). High-resolution thermodynamic measurements under pressure are typically challenging; however, using the present chemically tunable system, thermodynamic and entropic information near the metal-insulator boundary can be obtained by ambient-pressure heat capacity measurements. In this paper, we systematically investigated κ -[(BEDT-TTF) $_{1-x}$ (BEDT-STF) $_x$] $_2$ Cu $_2$ (CN) $_3$ by calorimetry to unveil thermodynamics features of the Mott transition between the potential QSL and FL states.

II. EXPERIMENT

Single crystals of the alloying compounds κ -[(BEDT-TTF) $_{1-x}$ (BEDT-STF) $_x$] $_2$ Cu $_2$ (CN) $_3$ are grown by the electrochemical oxidation method [37]. As shown in Table I, the crystal structural parameters were characterized by x-ray diffraction analyses, and the macroscopic homogeneity of the alloying crystals was confirmed. To evaluate the change in t'/t with mixing BEDT-STF molecules, we here introduce d'/d , the ratio of average dimer-dimer distance along the t' and t directions. The small changes in the lattice parameters within 0.5% were observed. Heat capacity measurements were carried out by a typical relaxation technique using a homemade thermal-relaxation-type calorimeter in a 3 He refrigerator with

TABLE I. Crystallographic data. F_w represents the formula weight for each sample. V shows the cell volume. Z denotes the number of formula units in the unit cell divided by the number of independent general positions. d'/d is the ratio of average dimer-dimer distance along the t' and t directions.

| x | 0.04 | 0.10 | 0.12 | 0.19 | 0.28 | 0.44 |
|-----------------------|----------|----------|----------|----------|----------|----------|
| F_w | 982.04 | 993.30 | 997.05 | 1010.18 | 1027.06 | 1057.07 |
| Space group | $P2_1/c$ | $P2_1/c$ | $P2_1/c$ | $P2_1/c$ | $P2_1/c$ | $P2_1/c$ |
| a (Å) | 16.1080 | 16.1054 | 16.1136 | 16.1569 | 16.1580 | 16.1761 |
| b (Å) | 8.5861 | 8.5816 | 8.5874 | 8.6000 | 8.6017 | 8.5982 |
| c (Å) | 13.3591 | 13.3751 | 13.3550 | 13.3663 | 13.3979 | 13.4037 |
| α (deg) | 90 | 90 | 90 | 90 | 90 | 90 |
| β (deg) | 113.691 | 113.565 | 113.66 | 113.519 | 113.551 | 113.208 |
| γ (deg) | 90 | 90 | 90 | 90 | 90 | 90 |
| V (Å ³) | 1691.9 | 1694.4 | 1692.6 | 1703.0 | 1707.0 | 1713.4 |
| Z | 2 | 2 | 2 | 2 | 2 | 2 |
| d'/d | 0.925 | 0.926 | 0.925 | 0.924 | 0.925 | 0.926 |

a 15-T superconducting magnet. The temperature range of these measurements is about 0.6–10 K. Magnetic fields were

applied perpendicular to the conducting plane. We measured the background data with a small amount of Apiezon N grease before mounting samples. These measurements were performed with single-crystalline samples weighing about 80–300 μg . The details of the calorimeter and experimental setup are reported in Ref. [40].

III. RESULTS

In Fig. 2, we present the temperature dependences of the heat capacity of the alloying system in a $C_p T^{-1}$ vs T^2 plot. The data in the temperature range up to 10 K are displayed in Fig. 2(a). There is only a subtle difference of about 6% at 10 K, mainly originating from the decrease in the Debye temperature induced by the Se substitution [41]. This means that the STF substitution induces only a small change of about a few percent in phonon contributions. In Fig. 2(b), the entropy S as a function of temperature is shown as a logarithmic plot. The entropy is calculated by integration of the experimentally obtained $C_p T^{-1}$ and the extrapolation down to 0 K estimated by polynomial fittings, and thus the calculated S includes the electronic and phonon contributions

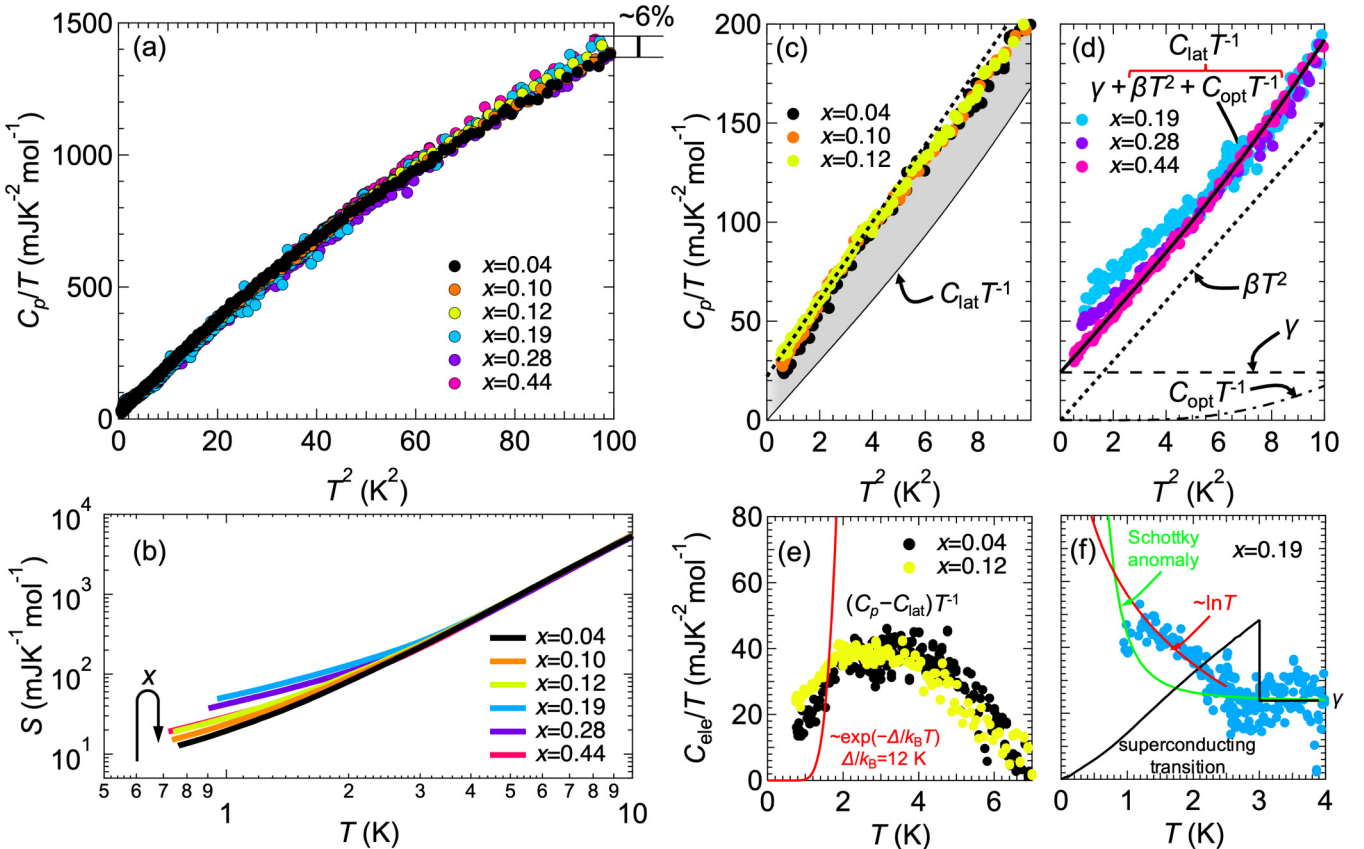


FIG. 2. (a) $C_p T^{-1}$ vs T^2 below 10 K for $x = 0.04$ – 0.44 . (b) Logarithmic plot of S as a function of temperature. (c) and (d) Enlarged plots of the low-temperature region below $T < 3.2$ K for $x < 0.15$ (c) and $x > 0.15$ (d). The dotted line in (c) is a fit to $C_p T^{-1} = \gamma + \beta T^2$ below 2 K for $x = 0.12$. The thin black curve in (c) is a rough estimate of lattice heat capacity $C_{\text{lat}} T^{-1}$ obtained from the FL salt ($x = 0.44$) by subtracting the γ term, which highlights the contribution of the low-energy excitations in the NMI state (shaded area). The black curves in (d) show the respective components of the fit of $C_p T^{-1} = \gamma + \beta T^2 + C_{\text{opt}} T^{-1}$ to the $x = 0.44$ data. (e) and (f) Electronic heat capacity $C_{\text{ele}} T^{-1}$ obtained by subtracting the lattice heat capacity $C_{\text{lat}} T^{-1}$ from the total $C_p T^{-1}$ for $x = 0.04$ and 0.12 (e) and $x = 0.19$ (f). The red curve in (e) shows activation-type gapped behavior when $\Delta/k_B = 12$ K. The red curve in (f) indicates a fit to $-\ln T$ while the black and green curves represent the typical superconducting and Schottky anomalies, respectively.

together. At higher temperatures, the x dependence of the entropy is small because the main portion of the total entropy is the phonon contribution. In the lower-temperature region, the $x = 0.19$ salt shows the larger entropy compared with the others. To shed light on the low-temperature region, the enlarged plots of $C_p T^{-1}$ below about 3.2 K ($= 10 \text{ K}^2$) are shown in Figs. 2(c) and 2(d). The data sets for $x < 0.15$ are shown in Fig. 2(c) while those for $x > 0.15$ are in Fig. 2(d) because the Mott insulating character in the low- x region changes into a metallic one across the boundary region at $x = 0.1\text{--}0.2$ according to previous reports [36,38,39]. The small change in lattice heat capacity indicates that the origin of the change observed in the low-temperature region should mainly come from the electronic contribution. In the case of typical metals having Fermi surfaces composed of itinerant electrons, $C_p T^{-1}$ at low temperatures obeys $C_p T^{-1} = \gamma + \beta T^2$, where γ and β represent the Sommerfeld coefficient of electronic heat capacity and the Debye coefficient of lattice heat capacity. Indeed, the $x = 0.44$ salt, which is deep inside the metallic FL region, shows a linear behavior below 2 K with $\gamma = 24.1 \text{ mJ K}^{-2} \text{ mol}^{-1}$ and $\beta = 15.0 \text{ mJ K}^{-4} \text{ mol}^{-1}$, which values are comparable to those of typical BEDT-TTF-based metallic salts [14,16,42]. Above 2 K, the behavior is gradually deviated by excess heat capacity that may originate from librational optical modes $C_{\text{opt}} \sim R(T_E/T) \exp(T_E/T) / [\exp(T_E/T) - 1]^2$, where T_E represents the Einstein temperature, as suggested for the other organic charge-transfer complexes with various structures [43].

On the other hand, the insulating salts shown in Fig. 2(d) do not share this behavior. At first glance, it appears to follow a linear behavior below 2 K, as indicated by the black dotted line. Also, the analysis of the data for $x = 0.04$ using the typical $C_p T^{-1} = \gamma + \beta T^2$ relation leads to $\gamma = 12.6 \text{ mJ K}^{-2} \text{ mol}^{-1}$ and $\beta = 21.2 \text{ mJ K}^{-4} \text{ mol}^{-1}$, which values are comparable to the previously reported $\gamma = 12 \text{ mJ K}^{-2} \text{ mol}^{-1}$ and $\beta = 21 \text{ mJ K}^{-4} \text{ mol}^{-1}$ for $x = 0$ [35]. However, above 2 K, the $C_p T^{-1}$ is lower than this linear dependence. Since higher-order terms of the Debye model appear only at higher temperatures, this behavior indicates that the Mott insulating state cannot be explained by the framework of the typical FL states. Nevertheless, the large low-temperature heat capacity in the insulating state proves the presence of low-energy spin excitations, which have been discussed as the finite γ and/or the relatively large β specific to the organic QSL state in previous works [35,44]. As a rough estimate, we show the lattice heat capacity $C_{\text{lat}} T^{-1}$, which is simply obtained by subtracting the γ term from the $x = 0.44$ data (the solid black curve), $C_p T^{-1} = \gamma + \beta T^2 + C_{\text{opt}}^{-1}$, as shown in Fig. 2(d). The difference from this estimate $(C_p - C_{\text{lat}}) T^{-1}$, which corresponds to the contribution of the spin excitations, is displayed as a $C_{\text{ele}} T^{-1}$ vs T plot in Fig. 2(e). This component does not appear to be a simple γ term. Electron spin resonance (ESR) results [34] suggest that the ground state is a gapped VBS state with a relatively large $\Delta/k_B \sim 12 \text{ K}$. However, the red curve, $\exp(-\Delta/k_B T)$ behavior for $\Delta/k_B = 12 \text{ K}$, does not describe the present results. Even if we assume that Δ/k_B is a variable parameter, it is difficult to reproduce the temperature dependence, and Δ/k_B must be extremely tiny. Including the present result, heat capacity measurements, sensitive to low-energy

excitations, indicate the presence of low-energy spin excitations, which is puzzling in view of a spin gap concluded from other measurements [34,45]. To clarify this point, experiments at lower temperatures seem necessary. Although the drop in the magnetic susceptibility below 6 K is observed, an exact zero susceptibility in a low-temperature limit has not been reported in these works [34]. To reconcile these arguments based on the temperature range of the measurements (ESR measurement above 2 K), one possibility is that the ground state has an incomplete spin gap, yielding some low-energy excitations, even below the putative transition at 6 K. Alternatively, an extrinsic origin, such as impurity spins or domain walls, was suggested to describe the low-temperature magnetic behavior [31,46]. However, it is unclear how to model the present temperature dependence with the suggested local orphan spins and local domain wall fluctuations, which may give the Schottky-type heat capacity and glasslike γT heat capacity, respectively.

For the $x = 0.19$ salt, located in the intermediate region [36,39], the temperature dependence [Fig. 2(d)] does not obey the $C_p T^{-1} = \gamma + \beta T^2$ relation due to the gradual upward deviation below $\sim 2.5 \text{ K}$. This behavior is clearer in the plot of $(C_p - C_{\text{lat}}) T^{-1}$, as shown in Fig. 2(f). Even though remnants of superconductive components are observed near the first-order Mott boundary of several κ -type salts, including some STF compounds [47], this behavior is completely distinct from the superconducting transition (the black curve). Furthermore, this deviation cannot be reproduced by an extrinsic Schottky anomaly arising from magnetic impurities (the green curve). In the case of the AFMI-FL Mott transition, such behavior is absent, and the simple $C_p T^{-1} = \gamma + \beta T^2$ relation is observed even very near the first-order Mott boundary [23,24,26]. The low-temperature gradual divergence is reminiscent of quantum critical behavior near a quantum critical point (QCP) because of the $-\ln T$ -like behavior (the red curve). Indeed, the present alloying system does not show significant first-order-like discontinuous behavior in our heat capacity data and resistivity data [36,38], albeit a dielectric catastrophe suggestive of phase inhomogeneity has been reported [39]. The first-order Mott transition observed in other κ -type salts is less obvious in κ -(BEDT-TTF)₂Cu₂(CN)₃; nevertheless, the weak first-order Mott transition with the critical endpoint located at 15–20 K has been observed in transport, nuclear magnetic resonance (NMR), and dielectric measurements [8,9,39]. A small difference between the alloying system and κ -(BEDT-TTF)₂Cu₂(CN)₃ may further lead to suppression of the remaining first-order nature. Randomness effects should also be taken into account, as a disorder can lower the temperature of the critical endpoint [48]. Regardless of the origin of the suppression of the first-order nature, the low-temperature diverging heat capacity indicates that quantum fluctuations are developed in this temperature region ($< 2.5 \text{ K}$). Since this behavior is significant at $x = 0.19$ and smaller at $x = 0.28$, the QCP should be located close to $x = 0.2$, which is not far from the reported position of the metal-insulator transition [36,38,39]. The magnetic field dependences of the heat capacity for $x = 0.04, 0.12, 0.19, 0.28,$ and 0.44 are shown in Fig. 3. The upper panels show the low-temperature region below 10 K^2 , while the lower ones display

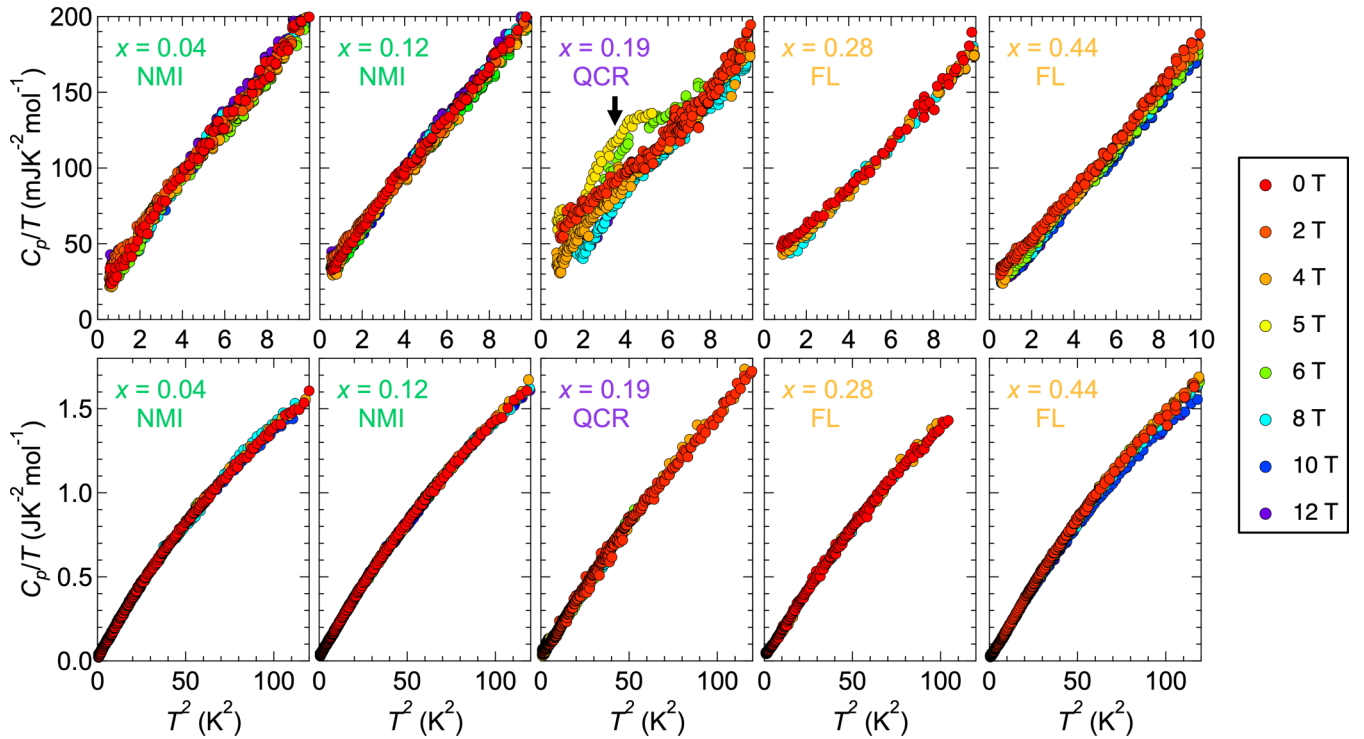


FIG. 3. $C_p T^{-1}$ vs T^2 at various magnetic fields for $x = 0.04$ and 0.12 for the NMI, $x = 0.19$ in the quantum critical region (QCR), and $x = 0.28$ and 0.44 for the FL. The upper panels show the data below 10 K^2 , while the lower ones show the data up to 120 K^2 . The arrow for the $x = 0.19$ data indicates a hump observed at fields of $5\text{--}6 \text{ T}$.

the data up to 120 K^2 . The fields are applied perpendicularly to the two-dimensional plane. For the NMI ($x = 0.04$) salt, the magnetic field dependence is not significant even at high magnetic fields. This fact indicates the robustness of these low-energy excitations against fields. However, the response to the magnetic field for the $x = 0.19$ sample, located in the quantum critical region (QCR), is distinct from those of the other salts. The upturn observed at 0 T disappears with increasing magnetic field, while a broad hump structure in the temperature dependence of $C_p T^{-1}$ appears at relatively high magnetic fields of $5\text{--}6 \text{ T}$. Since this behavior indicates that the low-temperature entropy shifts to higher temperatures in magnetic fields, the origin of this field dependence cannot be attributed to the 6-K anomaly and percolative superconductivity which is often observed near the first-order Mott transition. Considering the magnetic field dependence of the Mott boundary [23] and the bent quantum phase boundary [38,39] [Fig. 1(b)], the origin of the hump structure is also attributed to the critical behavior. By further increasing fields, the broad hump is also suppressed, and the field dependence is diminished. This behavior suggests that the high-field electronic state at low temperatures is out of the critical regime and can be regarded as the FL state.

IV. DISCUSSION

To deepen the understanding of the variations in the low-energy excitations around the Mott transition, we here show the low-temperature heat capacity at 1 K , $C_p(1 \text{ K})$, as a function of x in Fig. 4(a). In order to highlight the area near the Mott transition, each region is shown in a different

color in the figure. Based on the variation in γ depending on U/t [Fig. 1(c)], $C_p(1 \text{ K})$ should vary like the blue dashed curve if the Mott transition is between the AFMI and FL states. Namely, the deviation from the blue dashed curve is the peculiarity of the NMI-FL Mott transition. For the $x = 0.04$ salt, the value of $33.8 \text{ mJ K}^{-2} \text{ mol}^{-1}$, much larger than the $\beta = 15 \text{ mJ K}^{-4} \text{ mol}^{-1}$ for the $x = 0.44$ salt, suggests that the heat capacity involves finite low-energy excitations of the spin sector (the light blue double-headed arrow). With the approaching Mott transition, the $C_p(1 \text{ K})$ increases from the constant value in the NMI region. This behavior deviates from the blue dashed curve because γ is constantly zero inside the AFMI Mott phase. Upon crossing the boundary and entering the FL regime, $C_p(1 \text{ K})$ asymmetrically decreases and reaches $39.1 \text{ mJ K}^{-1} \text{ mol}^{-1}$ at $x = 0.44$, which is comparable to the typical value of $C_p(T = 1 \text{ K}) = \gamma + \beta$ for the BEDT-TTF-based metallic salts with $\gamma = 20\text{--}25 \text{ mJ K}^{-2} \text{ mol}^{-1}$ and $\beta = 10\text{--}15 \text{ mJ K}^{-4} \text{ mol}^{-1}$. The difference between the NMI and FL regions, shown by the pink double-headed arrow, should correspond to the contribution of the charge sectors of the π electrons, which is absent in the NMI state. If the inhomogeneity appearing near the first-order Mott transition develops around $x = 0.2$, the strong enhancement of $C_p(1 \text{ K})$ inside the FL region should not be observed near the boundary because the inhomogeneity significantly reduces the electronic heat capacity, as shown in Fig. 1(c).

Here, we examine the slope of the phase boundary between the NMI and FL states on the electronic phase diagram, dT/dx in Fig. 1(d). The positive slope indicates that the localization of electrons in the NMI state gives a larger entropy than the itinerancy of electrons in the FL state. This unusual

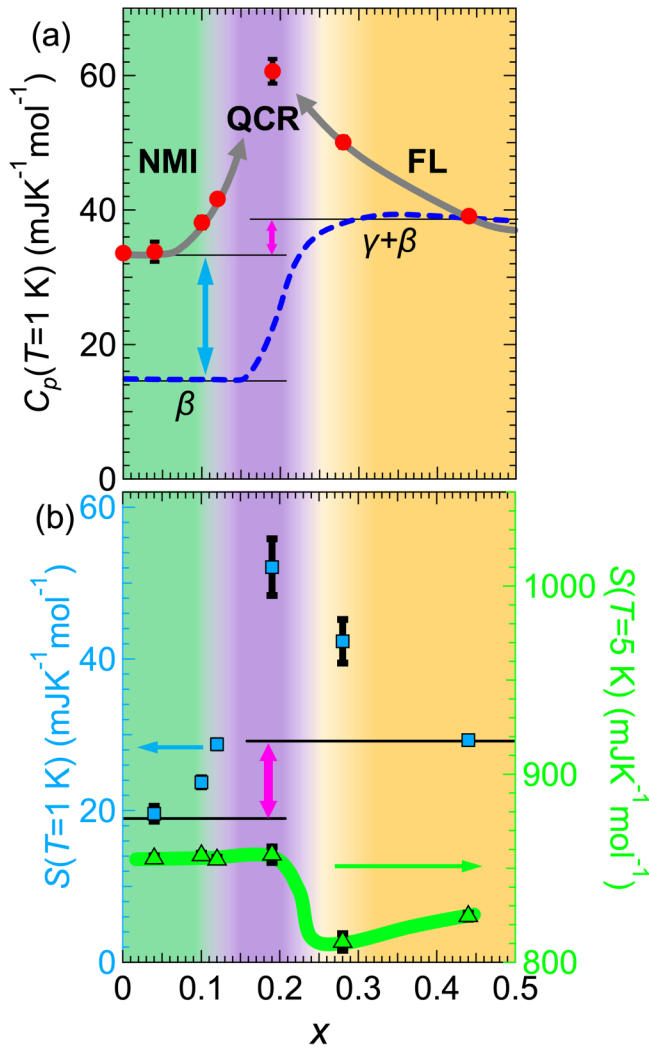


FIG. 4. Heat capacity C_p at 1 K (a) and entropy S at 1 K (left) and 5 K (right) (b) as a function of x . The blue dashed curve is the behavior expected based on the variation in γ for the Mott transition between the AFMI and FL states [Fig. 1(c)]. The light blue and pink arrows in (a) highlight the contribution of the spin and charge sectors in the electronic heat capacity of the FL state, respectively. The violet region represents the quantum critical region (QCR). The thick green curve superimposed on the data points in (b) is a visual guide to make the x dependence of $S(T = 5\text{ K})$ clearer.

behavior is reminiscent of the Pomeranchuk effect observed in ^3He , melting solid ^3He with lowering temperature through spin-lattice coupling [49,50]. In Fig. 4(b), we present the x dependence of the entropy S at 1 K (left axis) and 5 K (right axis). At 1 K, the entropy of the NMI state is lower than the entropy of the FL state. At 5 K, it is the opposite. As suggested by a theory [51], it is expected that there is only a small energy difference between the FL and Mott states because the gain in kinetic energy of electrons in the FL state is compensated by the loss in potential energy. In particular, when the frustration parameter t'/t is close to unity, the slope of the Mott boundary dU/dT is almost zero or a small negative value [52], and thus the energy difference between the two states should be very small. This delicate energy balance makes

the Mott transition winding on the phase diagram shown in Fig. 1(c). In real materials involving a variety of degrees of freedom, we must consider what the contribution is of an eventual factor determining how large or small the entropy is. The similar x dependence of $S(1\text{ K})$ and $C_p(1\text{ K})$ demonstrates that the low-temperature behavior can be explained by the electronic part and that the entropy of the NMI state is smaller at lower temperatures. However, at higher temperatures above 5 K, the lattice part must also be considered because the lattice components account for a large portion (>90%) of the total entropy in the soft organic crystal. To explain the reversal of the entropy appearing with elevating temperature, we need to discuss entropy originating from the phonons as well as the low-energy spin excitations. The characteristic of the present system is the confinement of the electrons in the triangular lattice making the antiferromagnetically interacting spins frustrated and disordered, which should result in lattice softening through the spin-lattice coupling. The lattice softening entails shifting the phonon density of states down to a lower-temperature region, as is observed in the NMI state. The presence of low-energy phonon excitations in the nonordered dimer-Mott triangular lattice system has been determined using thermal conductivity measurements [45], and therefore the softening of phonons can be a possible reason to explain the larger entropy in the NMI state. Nevertheless, another possibility is that the spin excitations explain the evolution of entropy with temperature in the NMI state. When dU/dT is negative, the entropy of the NMI state can become larger than that of the FL state. The formation of the possible nonmagnetic VBS ordered state [31,34] suggests a rapid increase in spin entropy with an enhancement of heat capacity near the transition temperature. This gap-closing behavior around 5 K may also relate to the reversal of the entropy. Although the spin entropy in the present system is not large, the relation may not be reversed even with the gain in the lattice entropy without the spin entropy. For the NMI system, the low-temperature Pomeranchuk-like phase boundary [53] is probably related to both contributions, namely, the phonon softening effect and spin contributions. To discuss these in more detail, knowledge of the temperature dependence of entropy up to higher temperatures is necessary.

We emphasize that the low-temperature heat capacity $C_p(1\text{ K})$ should reflect the variation of the ground state driven by quantum fluctuations predominantly. The gradual increase in $C_p(1\text{ K})$ with approaching the Mott boundary in the NMI phase suggests the continuous change in the low-energy excitations as the possible VBS state is suppressed near the Mott boundary. According to the correspondence between the chemical pressure characterized by x and physical pressure ($\Delta P = 1.5\text{ kbar}$ roughly corresponds to $\Delta x = 0.1$) [39] and the slope of the metal-insulator boundary $dx/dT \sim 2 \times 10^{-3}\text{ K}^{-1}$ (at $T = 5\text{ K}$), the Clausius-Clapeyron relation $dP/dT = \Delta S/\Delta V$ leads to the volume change $\Delta V \sim 2 \times 10^{-8}\text{ m}^3/\text{mol}$ with the entropy difference $\Delta S(5\text{ K}) \sim 50\text{ mJ K}^{-1} \text{mol}^{-1}$. Despite the rough estimation, the obtained ΔV is one order of magnitude smaller than the difference ΔV between $x = 0$ and $x = 0.1$, $\Delta V \sim 2 \times 10^{-7}\text{ m}^3/\text{mol}$ [36]. Thus, even if the boundary is a first-order transition, its discontinuity must be almost negligible. Near the QCP where the charge gap is just 0 K, quantum fluctuations related

to the instability of the charge itinerancy are enhanced and destabilize the quasiparticles characterizing the FL. It should be noticed that the quantum critical behavior is apparent only in the low-temperature region. It is worth noting that this energy scale is completely different from that of the high-temperature critical behavior induced by U and W , which is commonly observed in all dimer-Mott systems irrespective of the geometrical frustration [54]. Indeed, the low-temperature critical behavior is absent in the less-frustrated system κ -(d[n , n]-BEDT-TTF) $_2$ Cu[N(CN) $_2$]Br, which can access the first-order Mott transition between the AFMI and the FL states [23,24]. As the peculiarity of the NMI salt is the persistence of the low-energy excitations related to the spin part, the present critical behavior may be induced by the instability of the fractionalization of the electron into the spin and charge sectors. The present result and scenario agree with the discussion of a recent transport experiment under pressure [9] and a thermodynamic investigation of κ -[(BEDSe-TTF) $_x$ (BEDT-TTF) $_{1-x}$] $_2$ Cu[N(CN) $_2$]Br [55], which is also another candidate hosting the genuine Mott transition between the NMI and FL states, as well as theoretical works [29,30,56].

Finally, we briefly discuss the so-called “6-K anomaly” for the NMI sample, which has been discussed in a pristine $x = 0$ sample [31,35,57]. Although recent studies with high-quality samples and various sensitive measurements [34,58] have allowed us to get closer to the details of this anomaly, the details are still unclear because of some unresolved questions, such as the presence of the gapless excitations discussed above. Since the pristine salts reported in a previous work [35] were synthesized by other methods, their sample quality may differ from that of the present alloying series, and quantitative comparison may be challenging. Nevertheless, the systematic change in the physical parameters shown in Fig. 4 allows us to qualitatively compare our data with the results reported in the earlier work [35]. The data in Fig. 2(e) indicate that the anomaly seems to be broadened and suppressed down to 3–4 K for the $x = 0.04$ and 0.12 samples compared with that of the pristine sample. The black dots shown in Fig. 1(d) repre-

sent the x dependence of the peak temperature of the anomaly. Considering the relation to the charge disproportionation [59], it seems reasonable that the anomaly is smeared out by the suppression of the electron localization when approaching the Mott boundary. In the lower panels in Fig. 3, the magnetic field dependence of the anomaly is very small. This feature, which is robust against the magnetic field, is consistent with the estimation of a critical field of order 60 T for the pristine salt [31]. To elucidate this enigmatic anomaly, more detailed investigations are desired in future studies.

V. CONCLUSIONS

In summary, we report the low-temperature thermodynamic properties for the chemical pressure tuning system of the dimer-Mott compounds that show no long-range ordering even at low temperatures. The present result also provides evidence that the NMI state supports some gapless spin excitations. However, we also found that these low-energy excitations do not seem to be described by a simple FL-like γ term. The systematic change in the heat capacity depending on x revealed that the genuine Mott transition is potentially continuous via the QCP, which hosts the low-energy quantum fluctuations. In the NMI state, the lattice softening originating from the geometrically frustrated lattice gives the larger heat capacity in total, although the opening of the charge gap reduces the electronic heat capacity. Based on the entropy, the balance of these degrees of freedom makes a Pomeranchuk-like unique electronic phase diagram. The coupling of these degrees of freedom creates the low-temperature phase competition between the NMI and FL states, leading to the low-energy quantum critical behavior that may be related to the instability of the fractionalization of the electron into the spin and charge sectors.

ACKNOWLEDGMENT

This work was partially supported by JSPS KAKENHI Grants No. 19K22169 and No. 20H01862.

-
- [1] H. Kino and H. Fukuyama, Phase diagram of two-dimensional organic conductors: (BEDT-TTF) $_2$ X, *J. Phys. Soc. Jpn.* **65**, 2158 (1996).
 - [2] K. Kanoda, Metal-insulator transition in κ -(ET) $_2$ X and (DCNQI) $_2$ M: Two contrasting manifestation of electron correlation, *J. Phys. Soc. Jpn.* **75**, 051007 (2006).
 - [3] J. B. Powell and R. H. McKenzie, Strong electronic correlations in superconducting organic charge transfer salts, *J. Phys.: Condens. Matter* **18**, R827 (2006).
 - [4] F. N. Mott, The transition to the metallic state, *Philos. Mag.* **6**, 287 (1961).
 - [5] M. Imada, A. Fujimori, and Y. Tokura, Metal-insulator transitions, *Rev. Mod. Phys.* **70**, 1039 (1998).
 - [6] H. Morita, S. Watanabe, and M. Imada, Nonmagnetic insulating states near the Mott transitions on lattices with geometrical frustration and implications for κ -(ET) $_2$ Cu $_2$ (CN) $_3$, *J. Phys. Soc. Jpn.* **71**, 2109 (2002).
 - [7] B. Kyung and A.-M. S. Tremblay, Mott Transition, Antiferromagnetism, and d -Wave Superconductivity in Two-Dimensional Organic Conductors, *Phys. Rev. Lett.* **97**, 046402 (2006).
 - [8] Y. Kurosaki, Y. Shimizu, K. Miyagawa, K. Kanoda, and G. Saito, Mott Transition from a Spin Liquid to a Fermi Liquid in the Spin-Frustrated Organic Conductor κ -(ET) $_2$ Cu $_2$ (CN) $_3$, *Phys. Rev. Lett.* **95**, 177001 (2005).
 - [9] T. Furukawa, K. Kobashi, Y. Kurosaki, K. Miyagawa, and K. Kanoda, Quasi-continuous transition from a Fermi liquid to a spin liquid in κ -(ET) $_2$ Cu $_2$ (CN) $_3$, *Nat. Commun.* **9**, 307 (2018).
 - [10] F. Kagawa, K. Miyagawa, and K. Kanoda, Unconventional critical behaviour in a quasi-two-dimensional organic conductor, *Nature (London)* **436**, 534 (2005).
 - [11] S. Yasin, M. Dumm, B. Salameh, P. Batail, C. Mezère, and M. Dressel, Transport studies at the Mott

- transition of the two-dimensional organic metal κ -(BEDT-TTF)₂Cu[N(CN)₂]Br_xCl_{1-x}, *Eur. Phys. J. B* **79**, 383 (2011).
- [12] T. Sasaki, N. Yoneyama, and N. Kobayashi, Mott transition and superconductivity in the strongly correlated organic superconductor κ -(BEDT-TTF)₂Cu[N(CN)₂]Br, *Phys. Rev. B* **77**, 054505 (2008).
- [13] H. Watanabe, H. Seo, and S. Yunoki, Mechanism of superconductivity and electron-hole doping asymmetry in κ -type molecular conductors, *Nat. Commun.* **10**, 3167 (2019).
- [14] S. Imajo, K. Kindo, and Y. Nakazawa, Symmetry change of d -wave superconductivity in κ -type organic superconductors, *Phys. Rev. B* **103**, L060508 (2021).
- [15] D. Guterding, M. Altmeyer, H. O. Jeschke, and R. Valentí, Near-degeneracy of extended $s+d_{x^2-y^2}$ and d_{xy} order parameters in quasi-two-dimensional organic superconductors, *Phys. Rev. B* **94**, 024515 (2016).
- [16] S. Imajo, Y. Nakazawa, and K. Kindo, Superconducting phase diagram of the organic superconductor κ -(BEDT-TTF)₂Cu[N(CN)₂]Br above 30 T, *J. Phys. Soc. Jpn.* **87**, 123704 (2018).
- [17] S. Imajo, S. Yamashita, H. Akutsu, H. Kumagai, T. Kobayashi, A. Kawamoto, and Y. Nakazawa, Gap symmetry of the organic superconductor λ -(BETS)₂GaCl₄ determined by magnetic-field-angle-resolved heat capacity, *J. Phys. Soc. Jpn.* **88**, 023702 (2019).
- [18] A. Kawamoto, H. Taniguchi, and K. Kanoda, Superconductor-insulator transition controlled by partial deuteration in BEDT-TTF salt, *J. Am. Chem. Soc.* **120**, 10984 (1998).
- [19] H. Taniguchi, A. Kawamoto, and K. Kanoda, Superconductor-insulator phase transformation of partially deuterated κ -(BEDT-TTF)₂Cu[N(CN)₂]Br by control of the cooling rate, *Phys. Rev. B* **59**, 8424 (1999).
- [20] E. Gati, M. Garst, S. R. Manna, U. Tutsch, L. Bartosch, H. Schubert, T. Sasaki, A. J. Schlueter, and M. Lang, Breakdown of Hooke's law of elasticity at the Mott critical endpoint in an organic conductor, *Sci. Adv.* **2**, e1601646 (2016).
- [21] E. Gati, U. Tutsch, A. Naji, M. Garst, S. Köhler, H. Schubert, T. Sasaki, and M. Lang, Effects of disorder on the pressure-induced Mott transition in κ -(BEDT-TTF)₂Cu[N(CN)₂]Cl, *Crystals* **8**, 38 (2018).
- [22] D. Fournier, M. Poirier, M. Castonguay, and K. Truong, Mott Transition, Compressibility Divergence, and the P - T Phase Diagram of Layered Organic Superconductors: An Ultrasonic Investigation, *Phys. Rev. Lett.* **90**, 127002 (2003).
- [23] Y. Matsumura, S. Imajo, S. Yamashita, H. Akutsu, and Y. Nakazawa, Electronic heat capacity and lattice softening of partially deuterated compounds of κ -(BEDT-TTF)₂Cu[N(CN)₂]Br, *Crystals* **12**, 2 (2022).
- [24] Y. Nakazawa, H. Taniguchi, A. Kawamoto, and K. Kanoda, Electronic specific heat at the boundary region of the metal-insulator transition in the two-dimensional electronic system of κ -(BEDT-TTF)₂Cu[N(CN)₂]Br, *Phys. Rev. B* **61**, R16295(R) (2000).
- [25] J. Wosnitza, X. Liu, D. Schweitzer, and H. J. Keller, Specific heat of the organic superconductor κ -(BEDT-TTF)₂I₃, *Phys. Rev. B* **50**, 12747 (1994).
- [26] Y. Nakazawa and K. Kanoda, Electronic structure of insulating salts of the κ -(BEDT-TTF)₂X family studied by low-temperature specific-heat measurements, *Phys. Rev. B* **53**, R8875(R) (1996).
- [27] J. Vučićević, H. Terletska, D. Tanasković, and V. Dobrosavljević, Finite-temperature crossover and the quantum Widom line near the Mott transition, *Phys. Rev. B* **88**, 075143 (2013).
- [28] G. Sordi, P. Semon, K. Haule, and A.-M. S. Tremblay, Pseudogap temperature as a Widom line in doped Mott insulators, *Sci. Rep.* **2**, 547 (2012).
- [29] T. Senthil, Theory of a continuous Mott transition in two dimensions, *Phys. Rev. B* **78**, 045109 (2008).
- [30] W. Witczak-Krempa, P. Ghaemi, T. Senthil, and Y. B. Kim, Universal transport near a quantum critical Mott transition in two dimensions, *Phys. Rev. B* **86**, 245102 (2012).
- [31] A. Pustogow, Thirty-year anniversary of κ -(BEDT-TTF)₂Cu₂(CN)₃: Reconciling the spin gap in a spin-liquid candidate, *Solids* **3**, 93 (2022).
- [32] Y. Shimizu, K. Miyagawa, K. Kanoda, M. Maesato, and G. Saito, Spin Liquid State in an Organic Mott Insulator with a Triangular Lattice, *Phys. Rev. Lett.* **91**, 107001 (2003).
- [33] H. O. Jeschke, M. de Souza, R. Valentí, R. S. Manna, M. Lang, and J. A. Schlueter, Temperature dependence of structural and electronic properties of the spin-liquid candidate κ -(BEDT-TTF)₂Cu₂(CN)₃, *Phys. Rev. B* **85**, 035125 (2012).
- [34] B. Miksch, A. Pustogow, M. J. Rahim, A. A. Bardin, K. Kanoda, J. A. Schlueter, R. Hübner, M. Scheffler, and M. Dressel, Gapped magnetic ground state in quantum spin liquid candidate κ -(BEDT-TTF)₂Cu₂(CN)₃, *Science* **372**, 276 (2021).
- [35] S. Yamashita, Y. Nakazawa, M. Oguni, Y. Oshima, H. Nojiri, Y. Shimizu, K. Miyagawa, and K. Kanoda, Thermodynamic properties of a spin-1/2 spin-liquid state in a κ -type organic salt, *Nat. Phys.* **4**, 459 (2008).
- [36] Y. Saito, R. Rösslhuber, A. Löhle, M. Sanz Alonso, M. Wenzel, A. Kawamoto, A. Pustogow, and M. Dressel, Chemical tuning of molecular quantum materials κ -[(BEDT-TTF)_{1-x}(BEDT-STF)_x]₂Cu₂(CN)₃: from the Mott-insulating quantum spin liquid to metallic Fermi liquid, *J. Mater. Chem. C* **9**, 10841 (2021).
- [37] Y. Saito, T. Minamidate, A. Kawamoto, N. Matsunaga, and K. Nomura, Site-specific ¹³C NMR study on the locally distorted triangular lattice of the organic conductor κ -(BEDT-TTF)₂Cu₂(CN)₃, *Phys. Rev. B* **98**, 205141 (2018).
- [38] A. Pustogow, Y. Saito, A. Löhle, M. Sanz Alonso, A. Kawamoto, V. Dobrosavljevic, M. Dressel, and S. Fratini, Rise and fall of Landau quasiparticles while approaching the Mott transition, *Nat. Commun.* **12**, 1571 (2021).
- [39] A. Pustogow, R. Rösslhuber, Y. Tan, E. Uykur, A. Böhme, M. Wenzel, Y. Saito, A. Löhle, R. Hübner, A. Kawamoto, J. A. Schlueter, V. Dobrosavljevic, and M. Dressel, Low-temperature dielectric anomaly arising from electronic phase separation at the Mott insulator-metal transition, *npj Quantum Mater.* **6**, 9 (2021).
- [40] S. Imajo, S. Fukuoka, S. Yamashita, and Y. Nakazawa, Construction of relaxation calorimetry for 10¹⁻² μg samples and heat capacity measurements of organic complexes, *J. Therm. Anal. Calorim.* **123**, 1871 (2016).
- [41] E. S. R. Gopal, *Specific Heat at Low Temperatures* (Plenum, New York, 1966).
- [42] M. Sorai, Y. Nakazawa, M. Nakano, and Y. Miyazaki, Calorimetric investigation of phase transitions occurring in molecule-based magnets, *Chem. Rev.* **113**, PR41 (2013).

- [43] S. Wanka, J. Hagel, D. Beckmann, J. Wosnitzer, J. A. Schlueter, J. M. Williams, P. G. Nixon, R. W. Winter, and G. L. Gard, Specific heat and critical fields of the organic superconductor β'' -(BEDT-TTF)₂SF₃CH₂CF₂SO₃, *Phys. Rev. B* **57**, 3084 (1998).
- [44] Y. Nakazawa and S. Yamashita, Thermodynamics of a liquid-like spin state in molecule-based magnets with geometric frustrations, *Chem. Lett.* **42**, 1446 (2013).
- [45] M. Yamashita, N. Nakata, Y. Kasahara, T. Sasaki, N. Yoneyama, N. Kobayashi, S. Fujimoto, T. Shibauchi, and Y. Matsuda, Thermal-transport measurements in a quantum spin-liquid state of the frustrated triangular magnet κ -(BEDT-TTF)₂Cu₂(CN)₃, *Nat. Phys.* **5**, 44 (2009).
- [46] K. Riedl, R. Valentí, and S. M. Winter, Critical spin liquid versus valence-bond glass in a triangular-lattice organic antiferromagnet, *Nat. Commun.* **10**, 2561 (2019).
- [47] Y. Saito, A. Löhle, A. Kawamoto, A. Pustogow, and M. Dressel, Pressure-tuned superconducting dome in chemically-substituted κ -(BEDT-TTF)₂Cu₂(CN)₃, *Crystals* **11**, 817 (2021).
- [48] M. Urai, T. Furukawa, Y. Seki, K. Miyagawa, T. Sasaki, H. Taniguchi, and K. Kanoda, Disorder unveils Mott quantum criticality behind a first-order transition in the quasi-two-dimensional organic conductor κ -(ET)₂Cu[N(CN)₂]Cl, *Phys. Rev. B* **99**, 245139 (2019).
- [49] I. Pomeranchuk, On the theory of liquid He³, *Zh. Eksp. Teor. Fiz.* **20**, 919 (1950).
- [50] E. R. Grilly, Pressure-volume-temperature relations in liquid and solid ³He, *J. Low Temp. Phys.* **4**, 615 (1971).
- [51] M. J. Rozenberg, G. Kotliar, and X. Y. Zhang, Mott-Hubbard transition in infinite dimensions. II, *Phys. Rev. B* **49**, 10181 (1994).
- [52] H. T. Dang, X. Y. Xu, K.-S. Chen, Z. Y. Meng, and S. Wessel, Mott transition in the triangular lattice Hubbard model: A dynamical cluster approximation study, *Phys. Rev. B* **91**, 155101 (2015).
- [53] A. Pustogow, M. Bories, A. Löhle, R. Rösslhuber, E. Zhukova, B. Gorshunov, S. Tomić, J. A. Schlueter, R. Hübner, T. Hiramatsu, Y. Yoshida, G. Saito, R. Kato, T.-H. Lee, V. Dobrosavljević, S. Fratini, and M. Dressel, Quantum spin liquids unveil the genuine Mott state, *Nat. Mater.* **17**, 773 (2018).
- [54] T. Furukawa, K. Miyagawa, H. Taniguchi, R. Kato, and K. Kanoda, Quantum criticality of Mott transition in organic materials, *Nat. Phys.* **11**, 221 (2015).
- [55] S. Imajo, N. Kato, R. J. Marckwardt, E. Yesil, H. Akutsu, and Y. Nakazawa, Persistence of fermionic spin excitations through a genuine Mott transition in κ -type organics, *Phys. Rev. B* **105**, 125130 (2022).
- [56] R. V. Mishmash, I. González, R. G. Melko, O. I. Motrunich, and M. P. Fisher, Continuous Mott transition between a metal and a quantum spin liquid, *Phys. Rev. B* **91**, 235140 (2015).
- [57] M. de Souza and L. Bartosch, Probing the Mott physics in κ -(BEDT-TTF)₂X salts via thermal expansion, *J. Phys.: Condens. Matter* **27**, 053203 (2015).
- [58] R. S. Manna, S. Hartmann, E. Gati, J. A. Schlueter, M. de Souza, and M. Lang, Low-Temperature lattice effects in the spin-liquid candidate κ -(BEDT-TTF)₂Cu₂(CN)₃, *Crystals* **8**, 87 (2018).
- [59] T. Kobayashi, Q.-P. Ding, H. Taniguchi, K. Satoh, A. Kawamoto, and Y. Furukawa, Charge disproportionation in the spin-liquid candidate κ -(ET)₂Cu₂(CN)₃ at 6 K revealed by ⁶³Cu NQR measurements, *Phys. Rev. Res.* **2**, 042023(R) (2020).